applied sciences

MDPI

*Article*

# Geochemical Characteristics of Carbonates and Indicative Significance of the Sedimentary Environment Based on Carbon–Oxygen Isotopes and Trace Elements: Case Study of the Lower Ordovician Qiulitage Formation in Keping Area, Tarim Basin (NW China)

**Li-Xin Wang [1,2,3,†], Tian-Jia Liu [4,†], Hong-Ji Xiao [5], Hong-Xian Chu [1,3,6,*], Kun Yan [1,3], Qing-Tong Wang [1,3,*] and Wen-Qin Jiang [1,3]**

1 Yantai Center of Coastal Zone Geological Survey, China Geological Survey, Yantai 264004, China; wlxin@mail.cgs.gov.cn (L.-X.W.); yankun@mail.cgs.gov.cn (K.Y.); 3001200041@email.cugb.edu.cn (W.-Q.J.)
2 School of Environment, China University of Geosciences, Wuhan 430074, China
3 Ministry of Natural Resources Observation and Research Station of Land-Sea Interaction Field in the Yellow River Estuary, Yantai 264000, China
4 State Key Laboratory of Shale Oil and Gas Enrichment Mechanisms and Effective Development, Beijing 100083, China; liutianjia.syky@sinopec.com
5 School of Earth Sciences and Resources, China University of Geosciences, Beijing 100083, China; xiaohj2015@cugb.edu.cn
6 Laboratory for Marine Mineral Resources, Qingdao National Laboratory for Marine Science and Technology, Qingdao 266071, China
* Correspondence: chx-8@163.com (H.-X.C.); wangqingtong@sohu.com (Q.-T.W.)
† These authors contributed equally to this work.



**Citation:** Wang, L.-X.; Liu, T.-J.; Xiao, H.-J.; Chu, H.-X.; Yan, K.; Wang, Q.-T.; Jiang, W.-Q. Geochemical Characteristics of Carbonates and Indicative Significance of the Sedimentary Environment Based on Carbon–Oxygen Isotopes and Trace Elements: Case Study of the Lower Ordovician Qiulitage Formation in Keping Area, Tarim Basin (NW China). *Appl. Sci.* **2024**, *14*, 7885. https://doi.org/10.3390/app14177885

Academic Editor: Simone Morais

Received: 20 June 2024
Revised: 14 August 2024
Accepted: 17 August 2024
Published: 5 September 2024



**Abstract:** The carbonate rock of the Qiulitage Formation is a significant stratum for oil and gas exploration in the Tarim Basin. To elucidate its environmental characteristics, we conducted tests and analyses of trace elements, carbon, and oxygen isotopes of the carbonate rocks of the Qiulitage Formation in the Kekeqigankake section of the Keping area. The results reveal that $\delta^{13}C$ values range between −1.7‰ and 4.3‰, with an average value of 1.645‰. $\delta^{18}O$ values fluctuate from −11.4‰ to −6‰, with an average value of −8.2475‰. Z values (paleosalinity) vary from 120.33 to 131.67, significantly exceeding 120 with an average value of 126.52, indicating a marine sedimentary environment. Paleotemperature values (T) range from 12.75 to 29.09 °C, with an average value of 21.36 °C, suggesting warm climate conditions. The Sr/Ba (3.42~24.39) and Sr/Cu (57.5~560) ratios are elevated, while Th/U (<1.32) and V/Cr (0.989~1.70) ratios are reduced, suggesting that the Qiulitage Formation was deposited in an oxygen-rich, warm marine sedimentary environment with relatively high salinity.

**Keywords:** Tarim Basin; Qiulitage Formation; carbon and oxygen isotopes; trace element; sedimentary environment

## 1. Introduction

The Tarim Basin, spanning 56 × $10^4$ $km^2$ in northwestern China, ranks among the three principal Paleozoic marine sedimentary basins in the country [1]. This expansive diachronous basin has undergone varied tectonic regimes throughout its evolutionary history, transitioning from a Paleozoic intracratonic basin to Mesozoic–Cenozoic foreland basins [2,3]. Situated between the Paleozoic Central Asia and the Tethys tectonic belts, the Tarim Basin is bounded by the Tien Shan Mountains to the north, the Kunlun Mountains to the south, the Altun Mountains to the east, and the Pamirs to the west (Figure 1). Ongoing large-scale oil and gas exploration within the basin has unearthed significant fossil fuel reserves, with confirmed petroleum reserves of 120.65 × $10^8$ t and natural gas

volumes of 14.7 × $10^{12}$ $m^3$ [4], prompting an escalating research interest in this region. The Cambrian–Ordovician marine carbonate successions are notably prevalent in the Tarim Basin and represent a crucial stratigraphic horizon for oil and gas exploration. Notably, recent discoveries have been made in the Tahe-Lunnan and Tazhong large oil and gas fields within this formation [5]. Within the realm of carbonate successions, the Upper Cambrian–Lower Ordovician Qiulitage Formation has been established as a reservoir [6]. Consequently, comprehending the formation's depositional environment is essential for evaluating its resource potential. Prior research on the Lower Ordovician–Upper Qiulitage Formation has primarily concentrated on stratigraphic succession divisions [7], reservoir characteristics, and its formation mechanisms [6,8,9]. However, there has been a relative lack of focus on the analysis of its depositional environments. In this study, we conducted a systematic evaluation of carbon and oxygen stable isotopes, as well as trace element geochemistry of carbonate rocks in the Upper Qiulitage Formation, based on extensive field observation and sedimentary petrology. This will provide a theoretical perspective for future oil and gas explorations.

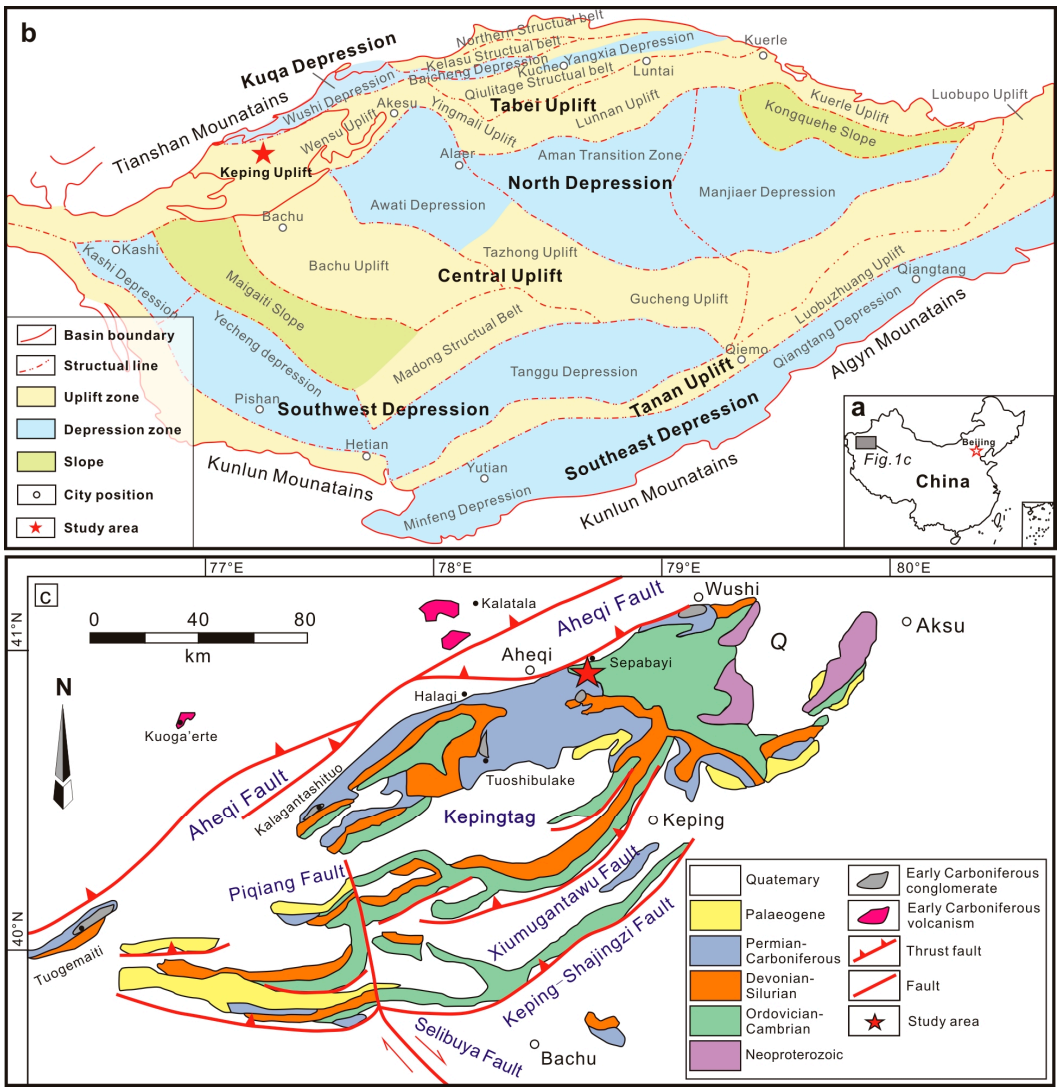


**Figure 1.** Location of the study area on a map of China (**a**). Structural units map of the Tarim Basin (**b**). Simplified geologic map of the Keping area (**c**) [10,11].

## 2. Geological Background

The Tarim Basin is tectonically distinguished by three primary uplifted regions and four significant depocenters, which can be further segmented into seven structural units:

the Tabei uplift, Central uplift, Tanan uplift, Kuqa depression, North depression, Southwest depression, and Southeast depression [12]. The Keping faulted uplift, the focus of this study, is located at the intersection of the Tien Shan orogenic belt and the northwest margin of the Tarim basin (Figure 1). This foreland fold-and-thrust belt consists of a series of NEE-striking imbricated overthrust nappes, formed by the collision of the Indian plate to the south and the Asian plate [13]. The Keping uplift is bordered by the Wushi sag and the South Tien Shan orogenic belt to the north, the Bachu positive relief and the Awati sag to the south, and is adjacent to the West Tian Shan fold-and-thrust belt to the west and the Wensu positive relief to the east (Figure 1). The Sepabayi area is characterized by outcropping Palaeozoic marine sedimentary rocks, including the Ordovician Qiulitag Formation, the Silurian Kepingtag and Tataaiertag Formations, the Devonian Yimugantaw Formation, the Carboniferous Bashisuogong and Biegentaw Formations, the Carboniferous-Permian Kangkelin Formation, and the Permian Kunkelaqi and Kalundaer Formations [10]. The study area is predominantly populated with Cambrian–Ordovician carbonates, notably the Upper Qiulitage Formation, which is triangular in shape and covers an approximate area of 5 $km^2$. This formation is thrust southward towards the Lower Silurian Kepingtage Formation and the Upper Carboniferous Bashisuogong Formation, while its northern region is enveloped by the Quaternary System. The stratum thickness of the Upper Qiulitage Formation in the outcropping Kekeqigankake section is approximately 864 m. The lithology primarily consists of dolomite, limestone, dolomitic limestone, and calcareous dolomite, interspersed with layers containing chert nodules and cephalopod fossils.

## 3. Analytical Methods

In this study, 40 whole rock samples were collected from fresh, unaltered, calcite vein-free layers of the Upper Qiulitage Formation in the Kekeqigankake section, Keping area, Tarim basin (GPS: 78°41′40.8″ N; 40°56′26.3″ E). The section is an outcrop. We used PM04-0-1 as the first sample at the bottom of the profile, sampling from the old to the new stratigraphic succession until we collected sample PM04-24-1 (Table 1). Due to the length of the profile, we started numbering from PM13-0-1, sampling in chronological order from old to new until PM13-16-1. The samples are limestone and dolomite. All the samples were surface-cleaned and dried, grounded to 200 meshes in an agate bowl [14], and then sieved and packed in paper sample bags. C and O isotope analyses for 40 powder samples were performed using MAT-253 Mass Spectrometer manufactured by Finnigan MAT at the Analytical Laboratory of Beijing Research Institute of Uranium Geology (BRIUG), Beijing, China. Whole rock trace-element concentrations were also determined in BRIUG for further selected 27 powder samples, using a Perkin Elmer Elan DRC-e Induced Coupled Plasma-Mass Spectrometer against primary standard solutions and validated against certified standard rock materials. The analytical precision was generally better than 5%.

**Table 1.** Analysis results of C and O isotopic values of carbonate rocks of the Upper Qiulitage Formation in Kekeqigankake section, Keping area.

| Sample No. | Lithology | $\delta^{13}C_{PDB}$ /‰ | $\delta^{18}O_{PDB}$ /‰ | $\delta^{18}O_{SMOW}$ /‰ | Z Value | T (°C) |
|---|---|---|---|---|---|---|
| PM04-0-1 | Arenaceous limestone | 2.6 | −8.8 | 21.9 | 128.24 | 24.79 |
| PM04-1-1 | Arenaceous limestone | 2.6 | −8.5 | 22.2 | 128.39 | 23.40 |
| PM04-2-1 | Arenaceous limestone | 1.6 | −8.2 | 22.4 | 126.49 | 22.04 |
| PM04-3-1 | Dolomitic limestone | 0.6 | −8.8 | 21.8 | 124.15 | 24.79 |
| PM04-4-1 | Dolomitic limestone | 2.3 | −9 | 21.6 | 127.53 | 25.73 |
| PM04-5-1 | Micrite limestone | 3.2 | −8.4 | 22.3 | 129.67 | 22.94 |
| PM04-6-1 | Dolomitic limestone | 3.4 | −8.9 | 21.7 | 129.83 | 25.26 |
| PM04-7-1 | Micrite limestone | 2.8 | −8.5 | 22.2 | 128.8 | 23.40 |
| PM04-8-1 | Arenaceous limestone | 4.3 | −8.9 | 21.7 | 131.67 | 25.26 |
| PM04-9-1 | Dolomitic limestone | 3.3 | −9.3 | 21.4 | 129.43 | 27.15 |
| PM04-10-1 | Micrite limestone | 3.6 | −9.7 | 20.9 | 129.84 | 29.09 |
| PM04-11-1 | Arenaceous limestone | 2.3 | −9.3 | 21.3 | 127.38 | 27.15 |

**Table 1.** *Cont.*

| Sample No. | Lithology | $\delta^{13}C_{PDB}$ /‰ | $\delta^{18}O_{PDB}$ /‰ | $\delta^{18}O_{SMOW}$ /‰ | Z Value | T (°C) |
|---|---|---|---|---|---|---|
| PM04-12-1 | Arenaceous limestone | 1.2 | −9.1 | 21.5 | 125.23 | 26.20 |
| PM04-13-1 | dolomite | 3.5 | −7.6 | 23 | 130.68 | 19.38 |
| PM04-14-1 | dolomite | 2 | −8.3 | 22.3 | 127.26 | 22.49 |
| PM04-15-1 | Dolomitic limestone | 2.1 | −9.5 | 21.1 | 126.87 | 28.12 |
| PM04-16-1 | Dolomitic limestone | 3.1 | −9 | 21.6 | 129.17 | 25.73 |
| PM04-17-1 | Dolomitic limestone | 2.7 | −9 | 21.6 | 128.35 | 25.73 |
| PM04-18-1 | Dolomitic limestone | 3.1 | −8 | 22.7 | 129.66 | 21.14 |
| PM04-20-1 | Dolomitic limestone | 3.1 | −9.8 | 20.8 | 128.77 | 29.58 |
| PM04-21-1 | Dolomitic limestone | 2 | −6.3 | 24.4 | 128.26 | 13.94 |
| PM04-22-1 | dolomite | 2 | −11.2 | 19.4 | 125.82 | 36.73 |
| PM04-23-1 | Dolomitic limestone | 3.2 | −10.7 | 19.9 | 128.53 | 34.12 |
| PM04-24-1 | Dolomitic limestone | 2.6 | −11.4 | 19.1 | 126.95 | 37.79 |
| PM13-0-1 | Limestone | 0.8 | −8.8 | 21.9 | 124.56 | 24.79 |
| PM13-1-1 | Limestone | −0.2 | −7.1 | 23.6 | 123.35 | 17.24 |
| PM13-2-1 | Limestone | 0.5 | −7.4 | 23.2 | 124.64 | 18.51 |
| PM13-3-1 | Limestone | 0.7 | −7.3 | 23.4 | 125.1 | 18.09 |
| PM13-4-1 | Limestone | 1.1 | −7.6 | 23.1 | 125.77 | 19.38 |
| PM13-5-1 | Limestone | 1.8 | −6.2 | 24.5 | 127.9 | 13.54 |
| PM13-6-1 | Limestone | −0.9 | −6.8 | 23.9 | 122.07 | 15.98 |
| PM13-7-1 | Limestone | −1.7 | −7 | 23.6 | 120.33 | 16.82 |
| PM13-8-1 | Limestone | −1.4 | −7.8 | 22.8 | 120.55 | 20.26 |
| PM13-9-1 | dolomite | −0.6 | −7.4 | 23.3 | 122.39 | 18.51 |
| PM13-10-1 | dolomite | 0.3 | −7.4 | 23.2 | 124.23 | 18.51 |
| PM13-11-1 | Dolomitic limestone | −0.7 | −6.5 | 24.2 | 122.63 | 14.75 |
| PM13-12-1 | dolomite | −0.2 | −7.1 | 23.5 | 123.35 | 17.24 |
| PM13-13-1 | Calcareous dolomite | 0.7 | −6 | 24.7 | 125.75 | 12.75 |
| PM13-14-1 | Dolomitic limestone | 0.5 | −7 | 23.7 | 124.84 | 16.82 |
| PM13-16-1 | Limestone | 1.9 | −6.3 | 24.4 | 128.05 | 13.94 |

## 4. Results

The bottom of the Lower part consists of grayish-black interbedded pelitic limestone intercalated with grayish-white layered chalky limestone. The middle is composed of gray layered chalky limestone interlayered with shallow gray thin to medium layered chalky limestone. The upper consists of gray layered argillaceous limestone that gradually transitions into shallow gray layered granular limestone with localized pyrite nodules and scarce fossils. The bottom of the Middle part consists of bluish-gray interbedded chalky and cherty limestone with pyrite bands. Grayish-white medium-thick layered chalky limestone intercalated with dark gray chalky limestone appears upward. The top consists of grayish-white thick layered chalky limestone and chalky limestone, with few fossils. The Upper part is characterized by grayish-black granular limestone, with localized pyrite bands.

The $\delta^{13}C$ and $\delta^{18}O$ values of the carbonate rocks from the Upper Qiulitage Formation are listed in Table 1. The $\delta^{13}$CVPDB values of carbonate samples range from −1.7‰ to 4.3‰, with a mean value of 1.645‰. At the same time, the $\delta^{18}O$ values range from −11.4‰ to −6‰, with a mean value of −8.2475‰. Both the $\delta^{13}C$ and $\delta^{18}O$ values exhibit significant variability, with both positive and negative $\delta^{13}C$ values being observed, suggesting the presence of a diverse range of sedimentary environments [15].

The concentrations of the trace elements of carbonate samples are listed in Table 2. The analytical results indicate that the Sr concentrations are ranging from 104 to 711 μg/g. Moreover, the relatively high concentrations of V varying from 1.7 to 8.54 μg/g are also recorded (Table 2). The concentrations of Cr, Cu, Th, U, and Ba range from 1.57 to 7.8 μg/g, from 0.46 to 4.91 μg/g, from 0.23 to 1.6 μg/g, from 0.34 to 2.27 μg/g, and from 15.4 to 57.8 μg/g, respectively.

**Table 2.** Analysis results of REE of the Upper Qiulitage Formation in Kekeqigankake section, Keping area.

| Sample No. | V | Cr | Cu | Sr | Th | U | Ba | Sr/Ba | Sr/Cu | Th/U | V/Cr |
|---|---|---|---|---|---|---|---|---|---|---|---|
| PM04-0-1 | 4.64 | 3.01 | 3.67 | 280 | 0.47 | 1.38 | 26.4 | 10.61 | 76.29 | 0.34 | 1.54 |
| PM04-1-1 | 3.39 | 2.35 | 1.84 | 254 | 0.41 | 0.61 | 23.8 | 10.67 | 138.04 | 0.67 | 1.44 |
| PM04-2-1 | 2.25 | 1.81 | 1.46 | 243 | 0.39 | 0.73 | 18.4 | 13.21 | 166.44 | 0.53 | 1.24 |
| PM04-3-1 | 4.2 | 3.22 | 2.17 | 191 | 0.83 | 0.85 | 19.5 | 9.79 | 88.02 | 0.98 | 1.30 |
| PM04-4-1 | 2.98 | 2.52 | 0.8 | 207 | 0.58 | 0.5 | 28 | 7.39 | 258.75 | 1.16 | 1.18 |
| PM04-5-1 | 2.17 | 2.08 | 1.21 | 125 | 0.45 | 0.49 | 23.7 | 5.27 | 103.31 | 0.92 | 1.04 |
| PM04-6-1 | 2.65 | 2.68 | 1.65 | 217 | 0.7 | 0.73 | 26.8 | 8.10 | 131.52 | 0.96 | 0.99 |
| PM04-7-1 | 5.62 | 2.43 | 3.23 | 207 | 0.52 | 0.56 | 26 | 7.96 | 64.09 | 0.93 | 2.31 |
| PM04-8-1 | 3.88 | 3.15 | 1.16 | 104 | 0.67 | 0.72 | 24.6 | 4.23 | 89.66 | 0.93 | 1.23 |
| PM04-9-1 | 1.7 | 1.57 | 0.74 | 288 | 0.34 | 0.74 | 15.7 | 18.34 | 389.19 | 0.46 | 1.08 |
| PM04-10-1 | 2.19 | 2.01 | 0.58 | 212 | 0.52 | 0.43 | 17.6 | 12.05 | 365.52 | 1.21 | 1.09 |
| PM04-11-1 | 2.09 | 2.06 | 0.46 | 216 | 0.23 | 1.09 | 16.3 | 13.25 | 469.57 | 0.21 | 1.01 |
| PM04-12-1 | 4.81 | 3.4 | 3.22 | 185 | 0.71 | 1.3 | 39.6 | 4.67 | 57.45 | 0.55 | 1.41 |
| PM04-13-1 | 4.88 | 3.55 | 1.21 | 142 | 0.78 | 0.88 | 41.5 | 3.42 | 117.36 | 0.89 | 1.37 |
| PM13-3-1 | 1.8 | 2.09 | 0.6 | 217 | 0.3 | 0.34 | 27.1 | 8.01 | 560 | 0.88 | 0.86 |
| PM13-4-1 | 3.72 | 3.74 | 3.62 | 336 | 0.64 | 0.68 | 53.6 | 6.27 | 88.67 | 0.94 | 0.99 |
| PM13-5-1 | 3.18 | 3.14 | 3.6 | 321 | 0.48 | 0.69 | 57.8 | 5.55 | 63.89 | 0.70 | 1.01 |
| PM13-6-1 | 5.39 | 3.26 | 1.17 | 230 | 0.79 | 1.12 | 15.4 | 14.94 | 242.74 | 0.71 | 1.65 |
| PM13-7-1 | 6 | 3.52 | 2.29 | 284 | 0.91 | 1.26 | 37.7 | 7.53 | 165.07 | 0.72 | 1.70 |
| PM13-8-1 | 2.44 | 1.67 | 1.42 | 378 | 0.39 | 1.17 | 15.5 | 24.39 | 264.79 | 0.33 | 1.46 |
| PM13-9-1 | 8.54 | 5.93 | 2.04 | 376 | 1.38 | 2.27 | 38.4 | 9.79 | 348.53 | 0.61 | 1.44 |
| PM13-10-1 | 3.9 | 3.51 | 4.91 | 711 | 0.81 | 0.7 | 32.4 | 21.94 | 92.26 | 1.16 | 1.11 |
| PM13-11-1 | 4.12 | 3.54 | 3.88 | 453 | 0.85 | 1.43 | 45.9 | 9.87 | 94.85 | 0.59 | 1.16 |
| PM13-12-1 | 4.53 | 3.91 | 1.78 | 368 | 0.93 | 0.9 | 19.5 | 18.87 | 215.73 | 1.03 | 1.16 |
| PM13-13-1 | 8.07 | 7.8 | 2.74 | 384 | 1.31 | 0.99 | 24 | 16.00 | 140.15 | 1.32 | 1.03 |
| PM13-14-1 | 7.62 | 5.89 | 2.1 | 368 | 1.6 | 1.49 | 43.6 | 8.44 | 175.24 | 1.07 | 1.29 |
| PM13-16-1 | 2.8 | 2.63 | 1.59 | 481 | 0.48 | 0.85 | 29 | 16.59 | 302.52 | 0.56 | 1.06 |

## 5. Discussion

Under certain conditions, the distribution of trace elements, changes in their content, the association between them, and the carbon and oxygen isotope composition can provide valuable insights into the evolution process of a sedimentary environment [16–20]. Therefore, the trace-element distribution patterns, concentration variations, and C-O isotope fractionation can reflect the evolution of the sedimentary environment under certain conditions.

### *5.1. Theoretical Consideration for Diagenetic Overprints*

Using the original C-O isotope compositions of carbonate to decipher depositional environments requires a thorough understanding of the effects of diagenesis. The $\delta^{18}O$ values of sedimentary carbonate are very sensitive to diagenetic alteration. On the one hand, if the $\delta^{18}O$ values are less than −10‰, it is likely that the primary isotopic signals of carbonate rocks have been highly altered and may no longer provide the original information of the sedimentary conditions [21]. On the other hand, if the $\delta^{18}O$ values range from −10‰ to −5‰, alternation may occur to variable degrees while depositional $\delta^{18}O$ composition can be preserved [21–23]. Moreover, the relationship between $\delta^{18}O$ and $\delta^{13}C$ values can also determine whether it is affected by diagenetic alteration or not: a high correlation between both isotope values represents later alternation between depositional and diagenetic signals, whereas data discreteness suggests primary fraction during precipitation of carbonate minerals [21,24,25]. The $\delta^{18}O$ values of the studied samples, except for PM04-22-1, PM04-23-1, and PM04-24-1, are mostly greater than −10‰. There is no apparent linear relationship between $\delta^{18}O$ and $\delta^{13}C$ values ($R^2$ = 0.296, Figure 2). It can be inferred that the samples are less affected by diagenetic alteration and can reflect the original information of carbonate precipitation. Therefore, it is reliable to analyze the sedimentary environment of the studied carbonate rocks by O and C isotopes.

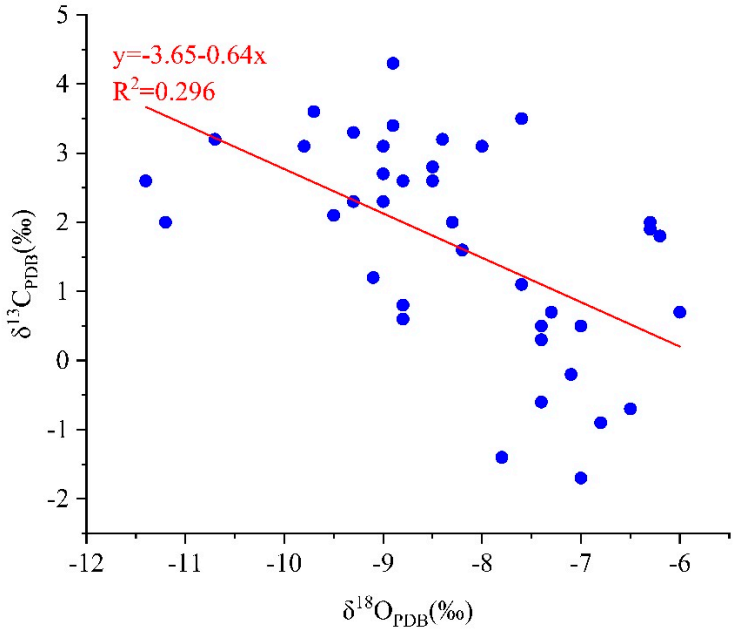


**Figure 2.** Scatter diagram shows the relationship between $\delta^{13}C$ and $\delta^{18}O$ of the carbonates of Upper Qiulitage Formation in Kekeqigankake section, Keping area. The blue dots represent each of the 40 samples analyzed and studied.

### *5.2. Paleosalinity Implications of Carbonate Rocks*

Based on the relationships between the salinity and $\delta^{13}C$ and $\delta^{18}O$ of carbonates [26,27], Keith and Weber proposed an empirical equation to calibrate the paleosalinity reconstruction [28], as expressed by:

$$Z = 2.048 \times (\delta^{13}C + 50) + 0.498 \times (\delta^{18}O + 50),$$

where Z represents the relative paleosalinity. For consistency, all isotopic compositions are expressed on the PDB scale. When $Z < 120$, the depositional environment is freshwater, whereas in the opposite case, the depositional environment is seawater. The equation has been widely and successfully used in the paleosalinity reconstruction of the strata in the Tarim Basin [29]. The Z values of the carbonate samples in this study range from 120.33 to 131.67, all greater than 120 (Table 2), which suggests that the carbonate rocks of the Upper Qiulitage Formation in the study area were formed in the carbonate platform of the marine environment.

The lithologic characteristics of the carbonate rocks in the Upper Qiulitage Formation suggest open or limited carbonate platform deposition. In the nearshore environment, a negative excursion of $\delta^{13}C$ values (from about 3‰ in the lower part to about 0‰ in the middle part) may indicate injection of a large amount of freshwater or rainwater, reduction in evaporation rates, and decrease in biological productivity [30]. The decreasing trend of $\delta^{13}C$ and Z values is shown in a few samples (the middle part of the middle part) in which Z values approach 120 (Figure 2). The oxygen isotope values become more positive from the middle part of the middle part to the top of the upper part. This could record an evaporation increase in the part.

In addition, Sr/Ba and Th/U values are also important indicators of paleosalinity [31–33]. The chemical behaviors of Sr and Ba are different in the supergene processes of fresh and seawater. In freshwater, both elements exist in the form of aqueous carbonate; when fresh water is mixed with seawater, the reaction of $Ba^{2+}$ and seawater-derived $SO_4^{2-}$ will form insoluble barite. Indeed, the tendency of Sr to be more enriched than Ba in seawater results in an increase in Sr/Ba ratios in carbonate materials as salinity increases [16,34]. Generally, the Sr/Ba value of freshwater sediment is less than one, while that of seawater sediment is greater than one [16]. Generally, an Sr/Cu value between 1 and 10 indicates a wet climate,

while >10.0 indicates a dry climate [35]. Generally, V/Cr values less than 2 suggest an aerobic environment, ranging from 2 to 4.25 suggest an anaerobic environment, while greater than 4.5 imply an anoxic environment [36]. The Sr/Ba values of 27 samples ranged from 3.42 to 24.39, with an average value of 11, indicating that the water salinity in the study area was high enough during the formation of the Upper Qiulitage Formation. It has been proposed by Tao et al. that when the Th/U value is less than seven [37], the carbonate is deposited in the marine environment. The maximum Th/U value of the carbonate rocks in this study is 1.32, indicating marine deposition, which is consistent with the result of the Sr/Ba indicator.

### 5.3. Paleoclimate Analysis of Carbonate Rocks

Urey found that the change in temperature will lead to variations of $\delta^{18}O/\delta^{16}O$ in carbonate rocks and proposed that it can be used as a geothermometer to determine the paleo-ocean temperature [38–40]. The formula for calculating paleotemperature by using oxygen isotopes was first proposed by Epstein in 1953 and further calibrated by Craig [41], as expressed by:

$$T = 16.9 - 4.2 \times (\delta^{18}O_c - \delta^{18}O_w) + 0.13 \times (\delta^{18}O_c - \delta^{18}O_w)^2$$

where $\delta^{18}O_c$ and $\delta^{18}O_w$ is the $\delta^{18}O_{PDB}$ value of $CO_2$ and the $\delta^{18}O_{SMOW}$ value of $H_2O$ generated by the reaction of $CaCO_3$ and $H_3PO_4$ at 25 °C.

The existence of the "age effect" requires further correction of the $\delta^{18}O$ values in carbonate rocks [28]. The average value of $\delta^{18}O$ in carbonate rocks in the Upper Qiulitage Formation is −8‰ after excluding three severely altered samples, compared with the value of −1.2‰ in Quaternary marine carbonate rocks. Thus, an average value of $\delta^{18}O = -6.8‰$ is to calibrate paleotemperature calculation formula as follows:

$$T = 16.9 - 4.2 \times (\delta^{18}O_{CaCO_3} + 0.22) + 0.13 \times (\delta^{18}O_{CaCO_3} + 0.22)^2$$

The calculation results show that the paleotemperature during sedimentation of the Upper Qiulitage Formation varies from 17.24 to 24.79 °C (Table 1), representing a warm-to-hot climate [42].

Among the trace elements in carbonate rocks, Cu concentration favors a wet environment, while Sr enrichment is an indicator of dry conditions, and Sr/Cu value is often used to reflect paleoclimates for carbonate precipitation [43]. The Sr/Cu values of the studied carbonate rocks are relatively high, ranging from 57.5 to 560, indicating that the carbonate rocks in the Upper Qiulitage Formation in the study area were formed in an arid climate. Moreover, the V/Cr value can also be used to determine the formation environment of carbonate rocks [44]. The V/Cr values of the samples collected in this study are mainly between 0.989 and 1.70, with an average value of 1.26, indicating that they were formed under oxidative conditions. In summary, the Upper Qiulitage Formation is deposited in a warm, aerobic, and arid environment.

### 5.4. Sea Level Variations during Carbonate Deposition

Carbon and oxygen isotopes of carbonate rocks are essential indicators of sea level fluctuations. When the sea level rises, the burial rate of organic carbon increases, causing the seawater $\delta^{13}C$ values to increase significantly [21,45].

The lithology characteristics and carbon and oxygen isotope results showed that the sea level frequently fluctuated during the deposition of the Upper Qiulitage Formation and experienced multiple transgressive–regressive cycles [12,46,47]. Grayish-black interbedded pelitic limestone intercalated with grayish-white layered chalky limestone in the lower part indicated the high sea level fluctuated in the period. The lower part of the Upper Qiulitage Formation was deposited during a regressive episode. Grayish-white medium-thick layered chalky limestone in the middle part displayed the low sea level stage. Grayish-black granular limestone in the upper part showed the sea level gradually rising. At the

early stage of the episode, the sea level fluctuated intermittently, and decreased slowly at the middle and late stages. As illustrated in Figure 3, the isotopic and chemical elemental ratios exhibit frequent fluctuations between 0 and 300 m of the logged section. Between 300 and 500 m of the logged section, only slight variations are observed in the oxygen isotopes, while the carbon isotopic composition and elemental ratios show a predominantly stable trend. The middle part experienced rapid transgressive–regressive episodes. In this part, the carbon isotopic composition reached its minimum value, while the ratios of Sr/Ba, Sr/Cu, and V/Cr also decreased to their lowest points. The sea level reached its lowest in the middle stage of the middle part and then slowly rose. The upper part generally inherited the transgression trend of the middle part, showing the characteristics of a rise in sea level. The carbon isotopic curve in this part showed an upward trend, while the Sr/Ba ratio in this segment was notably higher than that of the middle segment (Figure 3).

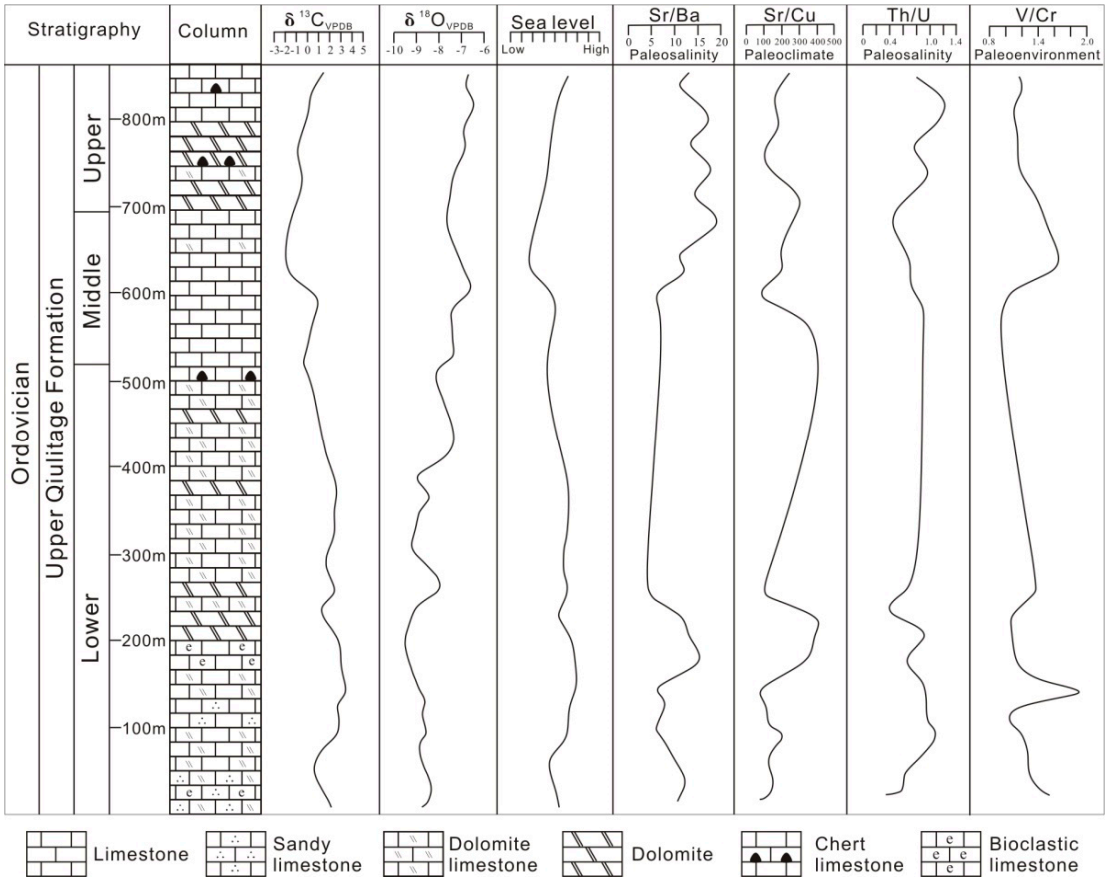


**Figure 3.** Stratigraphic distribution curves of $\delta^{13}C$–$\delta^{18}O$ and trace elements from the Upper Qiulitage Formation in Kekeqigankake section, Keping area.

## 6. Conclusions

Based on the comprehensive analyses of trace elements, carbon, and oxygen isotopes of carbonate rocks in the Lower Ordovician Upper Qiulitag Formation, the following conclusions are drawn:

(1) The carbonate lithology of the Upper Qiulitage Formation predominantly originated within the marine sedimentary milieu characterized by aerobic, thermally conducive, and relatively elevated salinity settings, potentially affording abundant organic matter conducive for the generation of hydrocarbon resources.

(2) Numerous transgressive and regressive episodes occurred during the depositional epoch of the Upper Qiulitage Formation.

(3) The lowermost and second segments of the initial interval of the Upper Qiulitage Formation, renowned for intense sea level fluctuations, may confer favorable spatial conditions for hydrocarbon production.

**Author Contributions:** Conceptualization, L.-X.W. and T.-J.L.; methodology, L.-X.W. and T.-J.L.; software, L.-X.W., T.-J.L. and H.-J.X.; validation, H.-X.C. and Q.-T.W.; formal analysis, L.-X.W. and T.-J.L.; investigation, W.-Q.J., Q.-T.W. and K.Y.; resources, Q.-T.W.; data curation, Q.-T.W.; writing—original draft preparation, L.-X.W., T.-J.L. and H.-J.X.; writing—review and editing, L.-X.W., T.-J.L. and W.-Q.J.; visualization, L.-X.W. and T.-J.L.; supervision, H.-X.C. and Q.-T.W.; project administration, Q.-T.W.; funding acquisition, H.-X.C. and Q.-T.W. All authors have read and agreed to the published version of the manuscript.

**Funding:** This research was funded by the China Geological Survey Project, numbers DD20243124, DD20211553, 1212011220661, and DD20160079.

**Institutional Review Board Statement:** Not applicable.

**Informed Consent Statement:** This article does not cover techniques used on humans.

**Data Availability Statement:** The original contributions presented in the study are included in the article, further inquiries can be directed to the corresponding author/s.

**Acknowledgments:** We thank our colleagues at Yantai Center of Coastal Zone Geological Survey, China Geological Survey, and China University of Geosciences, Beijing, for their field support, data analyses, constructive discussions, and comments.

**Conflicts of Interest:** The authors declare no conflicts of interest. The funders had no role in the design of the study; in the collection, analyses, or interpretation of data; in the writing of the manuscript, or in the decision to publish the results.

## References

1. Cao, Z.; You, D.; Qi, L.; Yun, L.; Hu, W.; Li, Z.; Qian, Y.; Liu, Y. New insights of the genesis of ultra-deep dolomite reservoirs in Well TS1, Tarim Basin: Evidence from in situ carbon and oxygen isotope analysis. *Nat. Gas Geosci.* **2020**, *31*, 915–922. (In Chinese with English abstract)
2. Lin, C.S.; Li, H.; Liu, J.Y. Major Unconformities, Tectonostratigraphic Frameword, and Evolution of the Superimposed Tarim Basin, Northwest China. *J. Earth Sci-China* **2012**, *23*, 395–407. [CrossRef]
3. Zhang, G.; Zhao, W.; Wang, H.; Li, H.; Liu, L. Multicycle tectonic evolution and composite petroleum systems in the Tarim Basin. *Oil Gas Geol.* **2007**, *28*, 653–663. (In Chinese with English abstract)
4. Kang, Y. The resource potential and exploration for oil and gas in the Tarim Basin. *Petrol. Sci. Bull.* **2018**, *3*, 369–375. (In Chinese with English abstract)
5. Zhang, G.; Liu, W.; Zhang, L.; Yu, B.; Li, H.; Zhang, B.; Wang, L. Cambrian-Ordovician prototypic basin, paleogeography and petroleum of Tarim Craton. *Earth Sci. Front.* **2015**, *22*, 269–276. (In Chinese with English abstract)
6. Zhang, C. Studies on Characteristics of Deep Carbonate Reserviors in the Yingshan-Xiaqiulitage Formations, Tahe Oilfield. Master's Thesis, Southwest Petroleum University, Chengdu, China, 2017. (In Chinese with English abstract)
7. Chen, Y.; Zhou, X.; Yang, H.; Pan, W.; Li, G. Sequence stratigraphy and its control on burial karstification dolostone reservoir in the Upper Cambrian Xiaqiulitage Formation at Xiao'Erbulake Section, Tarim Basin. *J. Stratigr.* **2010**, *34*, 77–82. (In Chinese with English abstract)
8. Zhu, H. Research on Genetic Mechanism and Key Controlling Factors of Xiaqiulitage Formation Reservoir in Bachu Region of Tarim Basin. Master's Thesis, Chengdu University of Technology, Chengdu, China, 2012. (In Chinese with English abstract).
9. Huang, L. Characteristics and Genetic Mechanism of the Dolomite Reservoir of Qiulitage Formation in Tazhong and Tabei Areas, Tarim Basin. Master's Thesis, China Universtiy of Geosciences (Beijing), Beijing, China, 2013. (In Chinese with English abstract)
10. Yu, H.; Qiu, K.; Pang, Y.; Zhao, Z.; Sun, Z.; Wen, Y. Early Carboniferous extension regime in South Tianshan: Constraints from alluvial fan of Bashisuogong Formation in Sepabayi area in Xinjiang, China. *Geol. J.* **2020**, *55*, 2902–2914. [CrossRef]
11. Zheng, J.; Huang, L.; Yuan, W.; Zhu, Y.; Qiao, Z. Geochemical features and its significance of sedimentary and diagenetic environment in the Lower Cambrian Xiaoerblak Formation of Keping area, Tarim Basin. *Nat. Gas Geosci.* **2020**, *31*, 698–709. (In Chinese with English abstract)
12. Zhang, Y.; Zhu, G.; Li, X.; Ai, Y.; Duan, P.; Liu, J. Resistance of eogenetic dolomites to geochemical resetting during diagenetic alteration: A case study of the lower Qiulitage Formation of the Late Cambrian, Tarim Basin. *Mar. Petrol. Geol.* **2024**, *164*, 106822. [CrossRef]
13. Yang, G. The analyses on NW-striking paleoplift and the hydrocarbon potential, northwest Tarim. *Xinjiang Geol.* **2003**, *21*, 157–162. (In Chinese with English abstract)

14. Jiang, W.; Chu, H.; Liu, Y.; Chen, B.; Feng, Y.; Lyu, J.; Yuan, J.; Wang, L.; Li, J.; Hou, W. Distribution of heavy metals in coastal sediments under the influence of multiple factors: A case study from the south coast of an industrialized harbor city (Tangshan, China). *Sci. Total Environ.* **2023**, *889*, 164208. [CrossRef] [PubMed]
15. Ye, F.H.; Zhao, L.S.; Zhang, L.; Cui, Y.; Algeo, T.J.; Chen, Z.Q.; Lyu, Z.; Huang, Y.; Bhat, G.M.; Aymon, B. Calcium isotopes reveal shelf acidification on southern Neotethyan margin during the Smithian-Spathian boundary cooling event. *Glob. Planet. Change.* **2023**, *227*, 104138. [CrossRef]
16. Deng, H.; Qian, K. *Sedimentary Geochemistry and Environmental Analysis*; Gansu Science and Technology Press: Lanzhou, China, 1993; pp. 95–104. (In Chinese)
17. Zhao, Z. *Principle of Trace Element Geochemistry*; Science Press: Beijing, China, 1997; pp. 183–204. (In Chinese)
18. Kontakiotis, G.; Karakitsios, V.; Cornée, J.; Moissette, P.; Zarkogiannis, S.D.; Pasadakis, N.; Koskeridou, E.; Manoutsoglou, E.; Drinia, H.; Antonarakou, A. Preliminary results based on geochemical sedimentary constraints on the hydrocarbon potential and depositional environment of a Messinian sub-salt mixed siliciclastic-carbonate succession onshore Crete (Plouti section, eastern Mediterranean). *Med. Geosc. Rev.* **2020**, *2*, 247–265. [CrossRef]
19. Kontakiotis, G.; Moforis, L.; Karakitsios, V.; Antonarakou, A. Sedimentary Facies Analysis, Reservoir Characteristics and Paleogeography Significance of the Early Jurassic to Eocene Carbonates in Epirus (Ionian Zone, Western Greece). *J. Mar. Sci. Eng.* **2020**, *8*, 706. [CrossRef]
20. Kontakiotis, G.; Karakitsios, V.; Maravelis, A.G.; Zarkogiannis, S.D.; Agiadi, K.; Antonarakou, A.; Pasadakis, N.; Zelilidis, A. Integrated isotopic and organic geochemical constraints on the depositional controls and source rock quality of the Neogene Kalamaki sedimentary successions (Zakynthos Island, Ionian Sea). *Med. Geosc. Rev.* **2021**, *3*, 193–217. [CrossRef]
21. Kaufman, A.J.; Knoll, A.H. Neoproterozoic variations in the C-isotopic composition of seawater: Stratigraphic and biogeochemical implications. *Precambrian Res.* **1995**, *73*, 27–49. [CrossRef] [PubMed]
22. Holland, G.; Saxton, J.M.; Lyon, I.C.; Turner, G. Negative $\delta^{18}O$ values in Allan Hills 84001 carbonate: Possible evidence for water precipitation on mars. *Geochim. Cosmochim. Acta* **2005**, *69*, 1359–1370. [CrossRef]
23. Grossman, E.L.; Joachimski, M.M. Ocean temperatures through the Phanerozoic reassessed. *Sci. Rep.* **2022**, *12*, 8938. [CrossRef]
24. Williams, D.F.; Lerche, I.; Full, W.E. *Isotope Chronostratigraphy: Theory and Methods*; Academic Press: San Diego, CA, USA, 1988; pp. 39–68.
25. Kaufman, A.J.; Jacobsen, S.B.; Knoll, A.H. The Vendian record of Sr and C isotopic variations in seawater: Implications for tectonics and paleoclimate. *Earth Planet. Sc. Lett.* **1993**, *120*, 409–430. [CrossRef]
26. Yang, M.; Yu, X.; Zhu, D.; Long, K.; Lu, C.; Zou, H. Depositional framework and reservoir characteristics of microbial carbonates in the fourth member of the middle Triassic Leikoupo Formation, western Sichuan Basin, South China. *Mar. Pet. Geol.* **2023**, *150*, 106113. [CrossRef]
27. Zhang, X.; Gao, Z.; Maselli, V.; Fan, T. Tectono-sedimentary characteristics and controlling factors of the lower-middle Cambrian gypsum-salt rocks in the Tarim Basin, Northwest China. *Mar. Pet. Geol.* **2023**, *151*, 106189. [CrossRef]
28. Keith, M.L.; Weber, J.N. Carbon and oxygen isotopic composition of selected limestones and fossils. *Geochim. Cosmochim. Acta* **1964**, *28*, 1787–1816. [CrossRef]
29. Zhu, J.; Yu, B.; Huang, W.; Chu, G.; Lv, G. Carbon and oxygen isotope features of Late Cambrian in central Tarim Basin. *Petrol. Geol. Oilfield Dev. Daqing* **2008**, *27*, 39–42. (In Chinese with English abstract)
30. Boggiani, P.C.; Gaucher, C.; Sial, A.N.; Babinski, M.; Simon, C.M.; Riccomini, C.; Valderez, P.F.; Thomas, R.F. Chemostratigraphy of the Tamengo Formation (Corumbá Group, Brazil): A contribution to the calibration of the Ediacaran carbon-isotope curve. *Precambrian Res.* **2010**, *182*, 382–401. [CrossRef]
31. Cao, L.; Zhang, Z.; Zhao, J.; Jin, X.; Li, H.; Li, J.; Wei, X. Discussion on the applicability of Th/U ratio for evaluating the paleoredox conditions of lacustrine basins. *Int. J. Coal Geol.* **2021**, *248*, 103868. [CrossRef]
32. Wang, A.; Wang, Z.; Liu, J.; Xu, N.; Li, H. The Sr/Ba ratio response to salinity in clastic sediments of the Yangtze River Delta. *Chem. Geol.* **2021**, *559*, 119923. [CrossRef]
33. Dashtgard, S.E.; Wang, A.; Pospelova, V.; Wang, P.; Croix, A.L.; Ayranci, K. Salinity indicators in sediment through the fluvial-to-marine transition (Fraser River, Canada). *Sci. Rep.* **2022**, *12*, 14303. [CrossRef]
34. Wang, A. Discriminant effect of sedimentary environment by the Sr/Ba ratio of different existing forms. *Acta Geol. Sin.* **1996**, *14*, 169–174. (In Chinese with English abstract)
35. Liu, G.; Zhou, D. Application of microelements analysis in identifying sedimentary environment-taking Qianjiang Formation in the Jianghan Basin as an example. *Petrol. Geol. Exp.* **2007**, *29*, 307–310+314. (In Chinese with abstract)
36. Jones, B.; Manning, D.A.C. Comparison of geochemical indices used for the interpretation of palaeoredox conditions in ancient mudstones. *Chem. Geol.* **1994**, *111*, 111–129. [CrossRef]
37. Tao, S.; Tang, D.; Zhou, C.; Li, F.; Li, Q.; Chen, X.; Meng, C. Element geochemical characteristics of the lower assemblage hydrocarbon source rocks in southeast Sichuan-central Guizhou (Chuandongnan-Qianzhong) region and its periphery areas and their implications to sedimentary environments. *Geol. China* **2009**, *36*, 397–403. (In Chinese with English abstract)
38. Urey, H.C. The thermodynamic properties of isotopic substances. *J. Chem. Soc.* **1947**, 562–581. [CrossRef] [PubMed]
39. Oehlert, A.M.; Swart, P.K. Rolling window regression of $\delta^{13}C$ and $\delta^{18}O$ values in carbonate sediments: Implications for source and diagenesis. *Depos. Rec.* **2019**, *5*, 613–630. [CrossRef]

40. Sharp, Z.D.; Wostbrock, J.A.G. Standardization for the Triple Oxygen Isotope System: Waters, Silicates, Carbonates, Air, and Sulfates. *Rev. Mineral. Geochem.* **2021**, *86*, 179–196. [CrossRef]
41. Craig, H. Standard for reporting concentrations of deuterium and oxygen-18 in natural waters. *Science* **1961**, *133*, 1833–1834. [CrossRef]
42. Scotese, C.R. An Atlas of Phanerozoic Paleogeographic Maps: The Seas Come in and the Seas Go Out. *Annu. Rev. Earth Planet. Sci.* **2021**, *49*, 679–728. [CrossRef]
43. Chen, Q.; Zhang, D.; Wang, J.; Zhao, F.; Liu, Y.; Zhang, Z.; Sun, X.; Huang, C.; Bai, Y. Geochemical characteristics of carbonate rocks in a salinized lacustrine basin: A case study from Oligocene formation in the Qaidam Basin, northwestern China. *Carbonates Evaporites* **2020**, *35*, 40. [CrossRef]
44. Yan, K.; Wang, C.L.; Mischke, S.; Wang, J.; Shen, L.; Yu, X.; Meng, L. Major and trace-element geochemistry of Late Cretaceous clastic rocks in the Jitai Basin, southeast China. *Sci. Rep.* **2021**, *11*, 13846. [CrossRef]
45. Hou, E.; Gao, J.; Wang, X.; Wang, G.; Hu, Q.; Ma, Z. Characteristics of carbon and oxygen isotopes of carbonate rocks in Riganpeicuo Formation of Upper Triassic in Renacuo area of Gaize, Tibet and its geological significance. *Geoscience* **2013**, *27*, 1332–1339. (In Chinese with English abstract)
46. Wang, H.; Gao, Z.; Machel, H.G.; Fan, T.; Duan, W. The Cambrian-Ordovician boundary in the Tarim Basin, NW China: Geochemistry and geophysics data anomalies. *J. Petrol. Sci. Eng.* **2017**, *156*, 497–512.
47. Zhang, Y.; Guo, Z.; Chen, D. Porosity distribution in cyclic dolomites of the Lower Qiulitag Group (Upper Cambrian) in northwestern Tarim Basin, China. *China Geol.* **2020**, *3*, 425–444.